nature geoscience

Article

https://doi.org/10.1038/s41561-024-01537-8

Indo-Pacific regional extremes aggravated by changes in tropical weather patterns

Received: 18 January 2024

Accepted: 20 August 2024

Published online: 4 October 2024

Check for updates

Chenyu Dong[1], Robin Noyelle[2], Gabriele Messori[3,4,5], Adriano Gualandi[6,7], Lucas Fery[2], Pascal Yiou[2], Mathieu Vrac[2], Fabio D'Andrea[8], Suzana J. Camargo[9], Erika Coppola[10], Gianpaolo Balsamo[11,12], Chen Chen[13], Davide Faranda[2,14] & Gianmarco Mengaldo[1]

The Pacific Walker circulation and the closely connected El Niño/Southern Oscillation influence the climate and weather of the tropical Indo-Pacific region. They specifically exert a strong control on the regional occurrence of weather extremes, such as heatwaves, heavy precipitation and prolonged dry spells, which are becoming increasingly frequent and severe. However, climate models struggle to accurately simulate large-scale circulation changes in the tropics and thus their consequences for regional weather and future climate. Here we use high-resolution ERA5 reanalysis data from 1940 to 2022 to study the occurrence trends of weather patterns in the tropical Indo-Pacific region. We find that new large-scale synoptic situations that were rarely present before the 1990s have emerged in the Indo-Pacific, while some others that were prominent have disappeared. Those new synoptic situations are associated with an unusual proportion of heatwaves and extreme precipitation in the region. These weather patterns are physically consistent with a trend towards a stronger Pacific Walker circulation, wetter and warmer conditions in Southeast Asia and drier conditions in the equatorial Pacific. These changes cannot be fully explained by El Niño/Southern Oscillation and other relevant modes of interannual variability, and other factors such as global warming, aerosol forcing, external forcing mechanisms and nonlinear mode interactions may be contributing.

Earth's climate is changing rapidly under the effect of global warming, leading to more frequent and severe extreme weather events in many regions[1]. The latter, in turn, exert heavy socioeconomic and environmental tolls[2–5]. A hotspot for changes in extreme events is the tropical Indo-Pacific, home to a large portion of the world's population and unique and vulnerable ecosystems. In this region, floods[6], heatwaves[7] and other extreme weather events[8] are becoming increasingly frequent and severe, leading to acute climate-change-induced distress[9–11].

Disentangling the mechanisms behind this increased frequency requires understanding the role of dynamical changes in regional weather patterns. Weather patterns can be understood as recurring spatial atmospheric configurations. Changes in these patterns are often harbingers of more frequent—and intense—extreme weather[1] and can amplify the effects of long-term thermodynamic trends[12,13].

Diagnosing robust changes in weather patterns and atmospheric dynamics under climate change is a long-standing challenge[14]. At the regional level, numerical models can present biases and show discrepancies with observations, and the signal in the observational record is often overshadowed by natural variability[15]. The Indo-Pacific presents additional, unique challenges in this context due to unexplained trends in the Pacific Walker circulation (PWC), the most prominent driver of weather and climate in the region[16–18].

The PWC is a zonal atmospheric circulation over the tropical Pacific. It consists of rising air motion over Southeast Asia and

A full list of affiliations appears at the end of the paper. e-mail: mpegim@nus.edu.sg

its surrounding oceans—the eastern Indian Ocean and the western Pacific—and descending air motion over the eastern Pacific. The PWC is modulated by the El Niño/Southern Oscillation (ENSO) and has a pronounced effect on global weather. Observations point to PWC strengthening in recent decades[17–20]. However, most models in the Coupled Model Intercomparison Project phases 5 and 6 are unable to capture this observed strengthening[16,18,20,21], possibly because of a cold-tongue bias in the Pacific[22]. This hinders understanding the observed changes in regional weather and extremes, and fuels uncertainty in their future projections[23–25]. Therefore, achieving a more comprehensive understanding of the changes in weather patterns in the tropical Indo-Pacific region over the past few decades, and their implications for weather extremes, is of crucial importance.

In this study, we analyse changes in atmospheric weather patterns in the tropical Indo-Pacific through the lens of newly developed approaches for studying recurrent weather patterns and their occurrence trends (Methods)[12,26]. These methods are commonly applied in the study of mid-latitude circulation but are rarely used in the study of atmospheric circulation in tropical regions[27]. We use 83 years of the state-of-the-art high-resolution ERA5 (fifth-generation European Centre for Medium-Range Weather Forecasts atmospheric reanalysis) reanalysis data[28] for the main analysis and identify similar patterns with significant occurrence trends in other reanalysis datasets—JRA55[29], NCEP[30], ERA-20C[31] and 20CR[32]—thereby demonstrating the robustness of our study. We find that, in recent years, certain weather patterns are emerging, and certain others are disappearing. The emerging patterns lead to highly coherent anomalies exhibiting a stronger PWC, more prevalent wet conditions in Southeast Asia and drier conditions in the equatorial Pacific. In addition, we find that these emerging weather patterns are considerably exacerbating extreme precipitation and heatwaves in the tropical Indo-Pacific, with a spatial footprint resembling, to a certain extent, that of La Niña (also referred to as the cold phase of ENSO). In agreement with recent studies, we find that the occurrence trends in weather patterns are not fully attributable to ENSO-driven variability[33], or to other relevant modes of variability, namely, Indian Ocean dipole (IOD)[34], Pacific decadal oscillation (PDO)[35] and Atlantic multidecadal oscillation (AMO)[36], although we are not able to conclusively attribute them to global warming trends or other external forcing mechanisms.

Emerging and disappearing weather patterns

The literature has commonly focused on the shifting mean state of regional weather patterns[20,37], namely, sets of similar synoptic circulations. Changes in such patterns can be used to diagnose low-frequency atmospheric changes. In this study, we instead identify analogues (sets of weather patterns similar to each other) and use them to quantify the occurrence trends of all individual weather patterns. That is, we obtain an occurrence trend for the spatial atmospheric pattern of each data timestep (day) we analyse in the Indo-Pacific region (50° E–120° W, 20° S–20° N)[12]. This means identifying the weather patterns that are closest to each other under Euclidean distance (analogues) in 83 years of ERA5 data (1940–2022[28]). We then divide the dataset into nine periods of equal duration and calculate the number of analogues for each period. If the number of analogues of a given weather pattern is increasing (decreasing) over time beyond a certain confidence interval, the weather pattern is emerging (disappearing). Emerging patterns can be seen as weather patterns that were rare in the distant past and that are now appearing more frequently, with the opposite applying to disappearing patterns. We focus on a relatively narrow tropical band since analogues-based methods may not perform as well if the region under study is too broad and encompasses too many climate systems. However, we conducted a sensitivity analysis on the studied domain, and as shown in Supplementary Fig. 3, it yielded consistent results despite identifying fewer patterns with trends. Full details are provided in Methods.

We define analogues using total column water vapour (TCWV) as the observed variable. TCWV is a key component of the water cycle in tropical regions[38] and contains information on both atmospheric dynamics (associated with atmospheric circulation) and thermodynamics (associated with temperature), including convection. TCWV further correlates directly to extremes such as heavy precipitation and prolonged dry conditions. We additionally analyse variables accounting for different atmospheric processes in the tropics (Extended Data Table 1).

Using TCWV, we identified 280 (0.92%) patterns with increasing occurrence trend (also referred to as emerging patterns) and 6,226 (20.54%) with decreasing occurrence trend (also referred to as disappearing patterns), out of a total of 30,316 possible weather states (number of timesteps in the dataset).

The detrended and deseasonalized composite anomaly maps for the days associated with emerging or disappearing patterns (Fig. 1a–h) show coherent regional anomalies with generally mirrored signs in TCWV, 850 hPa streamfunction (also referred to as 850 hPa-S), horizontal wind, total precipitation and 2 m temperature. The emerging weather patterns display increased precipitation and hotter weather over Southeast Asia and parts of Northern Australia, and less water vapour, decreased precipitation and colder weather over the equatorial Central Pacific (Fig. 1a,b,e–h). We also find stronger trade winds and a stronger PWC (Fig. 1c,d). The opposite is observed for the disappearing patterns.

The emerging patterns are clustered within the past 20–30 years of data. They exhibit a distinct seasonality, with the majority appearing between October and January (Fig. 1i). Disappearing patterns, instead, occur throughout the year and are clustered in the period 1940–1970, although some occur sporadically in recent decades (Fig. 1j). The emerging patterns exhibit an increasing trend of 11 analogues per decade (Fig. 1k), while the disappearing patterns exhibit a decreasing trend of 15 analogues per decade (Fig. 1l). This means that weather patterns that were once extremely rare have emerged in the past two decades, whereas those that previously accounted for a substantial proportion have become exceptionally rare. More importantly, these patterns are not random but exhibit highly coherent anomalies. The results in Fig. 1 are robust to the observable chosen (Extended Data Figs. 2 and 3), to the choice of periods used for computing the trends (Extended Data Fig. 4), to the duration of the dataset used (Extended Data Fig. 7), to the reanalysis dataset adopted (Extended Data Figs. 5 and 6 and Supplementary Figs. 1 and 2) and to the domain used (Supplementary Fig. 3), substantiating the results found.

The spatially coherent anomaly maps of emerging and disappearing weather patterns shown in Fig. 1 highlight a stronger PWC and resemble, to a certain extent, La Niña-like conditions (Extended Data Fig. 1). This suggests spatially coherent changes in the tropical dynamics that can impact weather extremes. Indeed, if we take a dynamical viewpoint, and consider the 850 hPa and 200 hPa streamfunctions as the observables (Extended Data Figs. 2 and 3; computed using the method in ref. 39), the composite anomalies show consistent results with TCWV anomalies, which also highlight a stronger PWC.

Impact on weather extremes

Whether and how the changes in tropical dynamics just presented impact extreme weather remains an open question. We focus on three high-impact extremes in the region: heatwaves, extreme precipitation and consecutive dry days (see Methods for more details on how these are identified). We restrict our analysis to the period 1979–2022 and focus on Southeast Asia (including Papua New Guinea, Solomon Islands and Vanuatu), Northern Australia and Southern India. This region is one of the most densely populated in the world (with an approximate total population of 1 billion people), and it is at the intersection of crucial shipping routes, factors that underscore its importance. In addition, we choose a shorter period (1979–2022) as opposed to the entire time

https://doi.org/10.1038/s41561-024-01537-8

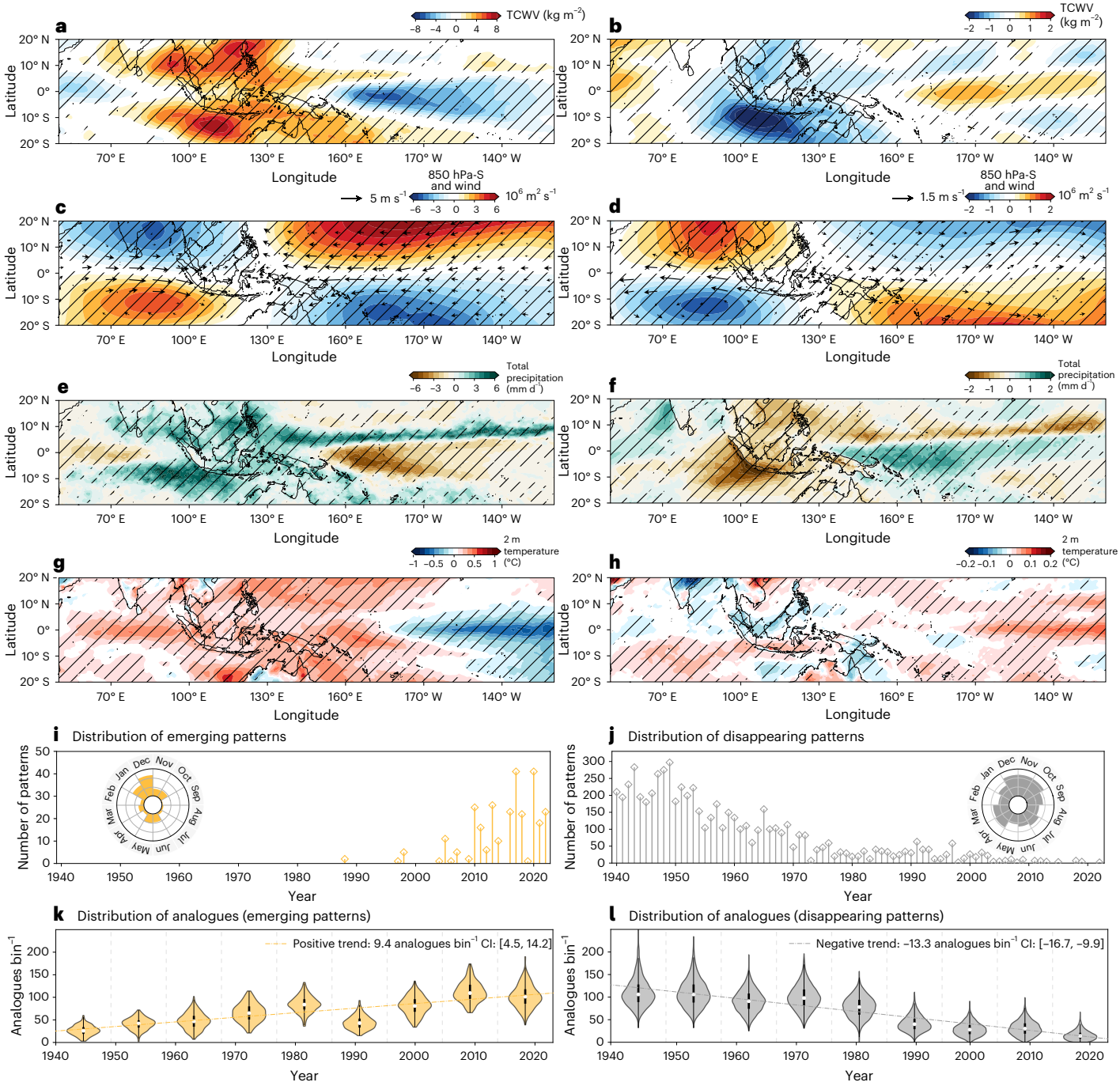

Fig. 1 | Composite anomalies for patterns with significant occurrence trends and associated analogues using TCWV as observable. a,**c**,**e**,**g**, Composite anomalies for emerging weather patterns. **b**,**d**,**f**,**h**, Composite anomalies for disappearing weather patterns. Diagonal black lines indicate regions with changes that are statistically significant at the one-sided 5% level, computed with a bootstrap sample size of 500. **i**,**j**, The number per year and seasonal distribution of patterns with increasing and decreasing occurrence trends, respectively. **k**,**l**, The count of analogues for emerging and disappearing patterns, respectively, in each period (each violin plot). The ends of the boxes represent the 25th and 75th percentiles, with the whiskers extending to 1.5 times the interquartile range beyond the box. The white dot in each box shows the median (n = 280 for emerging patterns; n = 6,226 for disappearing patterns). The dashed lines indicate the trend of the average count of analogues. CI, confidence interval.

history available in the ERA5 dataset (1940–2022) as there are no emerging patterns in previous decades.

Figure 2 shows the frequency ratio of weather extremes linked to the emerging (Fig. 2a,c,e) and disappearing (Fig. 2b,d,f) weather patterns identified in this study for the December–January–February (DJF)) season. The frequency ratio is computed as the ratio between the frequency of extremes appearing during the emerging patterns identified and the frequency of extremes appearing in climatology in the period 1979–2022 (see Methods for more details). Values greater than 1 indicate increased frequency compared with climatology. Values smaller than 1 indicate decreased frequency. For example, a value of 2 indicates that an extreme striking during the emerging patterns is twice as likely compared with climatology. In the Supplementary Information, we provide the same analysis for the other three seasons as well

https://doi.org/10.1038/s41561-024-01537-8

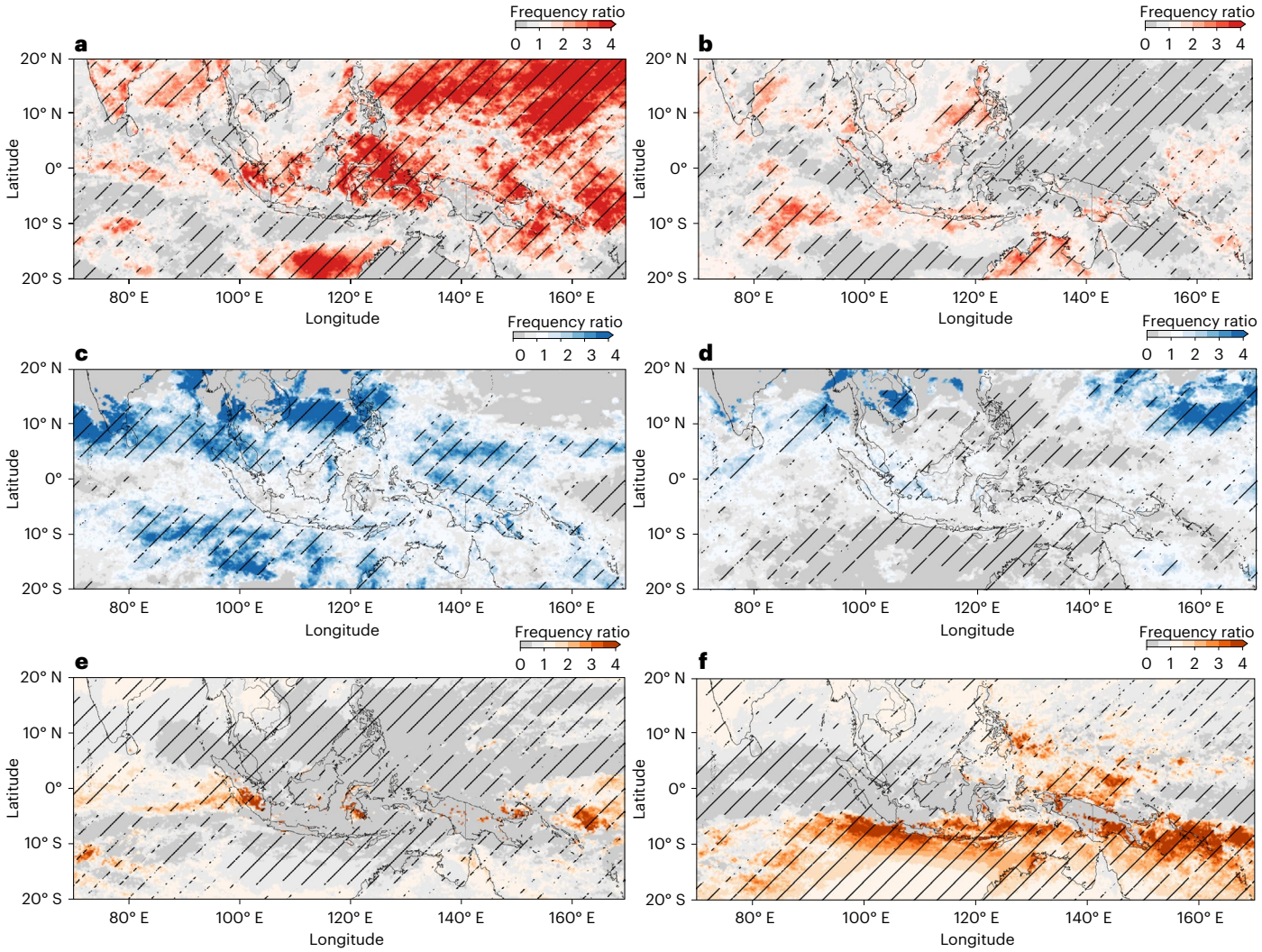

Fig. 2 | Weather extremes associated with emerging and disappearing weather patterns in DJF. a–**f**, Frequency ratio maps for heatwaves (**a**,**b**), extreme precipitation (**c**,**d**) and consecutive dry days (**e**,**f**) (Methods) as associated with emerging (**a**,**c**,**e**) and disappearing (**b**,**d**,**f**) weather patterns in DJF. Diagonal black lines indicate regions with changes that are statistically significant at the one-sided 5% level, computed with a bootstrap sample size of 500. Vertical bars on the bottom left corner show the average frequency of climatology (grey bar) versus emerging and disappearing patterns (coloured bars).

as whole-year results without separation into seasons (Supplementary Figs. 4–7). In the Supplementary Information, we also provide two tables (Supplementary Tables 1 and 2) that detail the frequency across the four seasons considered and for ocean only, for land only and for eight different land regions.

We find that heatwaves and extreme precipitation exhibit an increased frequency when associated with the emerging weather patterns identified, with specific coherent spatial patterns, for the DJF season. For example, several regions in Indonesia (including Central Sumatra, West Borneo and Sulawesi), South Myanmar and South India, as well as the Bay of Bengal and the western Pacific, exhibit markedly increased frequency of heatwaves compared with climatology (Fig. 2a). The South China Sea and its surrounding areas (including Vietnam and the Philippines), the Malay Peninsula, the tip of South India and a portion of the Indian Ocean off the coast of Australia exhibit considerably increased frequency of extreme precipitation, while an increased frequency is observed in other portions of Southeast Asia and the tropical Western Pacific (Fig. 2c). For consecutive dry days, there is an overall decrease for the emerging patterns compared with climatology, albeit some regions, including Central Indochina and Central Sumatra, experience an increased frequency (Fig. 2e). The results for disappearing weather patterns (Fig. 2b,d,f) mirror those obtained for emerging weather patterns, corroborating the findings.

To complement the analysis, we link the results obtained on weather extremes to flooding events recorded in the Emergency Events Database (EM-DAT)[40] for the DJF season (Fig. 3a,b). The use of EM-DAT comes with some obvious caveats: only events with high social impact are recorded in the database, and reporting may suffer from both spatial and temporal inaccuracy, particularly in the early part of the dataset[41] and data-scarce regions such as Southeast Asia. We note that a similar analyses were not possible for heatwaves and consecutive dry days as there are not enough recorded events in EM-DAT for the region of interest. We observe that the emerging patterns are strongly associated with floods (77/130 = 59.2%) compared with the overall frequency of flooding days (886/3,971 = 22.3%). More specifically, countries with a higher frequency ratio of flooding days (including Vietnam, Thailand, Malaysia, Sri Lanka and the Philippines) exhibit a higher frequency ratio of extreme precipitation days in Fig. 2g. Results for the other three seasons are reported in Supplementary Figs. 8–10. Despite potential inaccuracies and insufficient historical data, EM-DAT corroborates the results obtained using reanalysis data.

https://doi.org/10.1038/s41561-024-01537-8

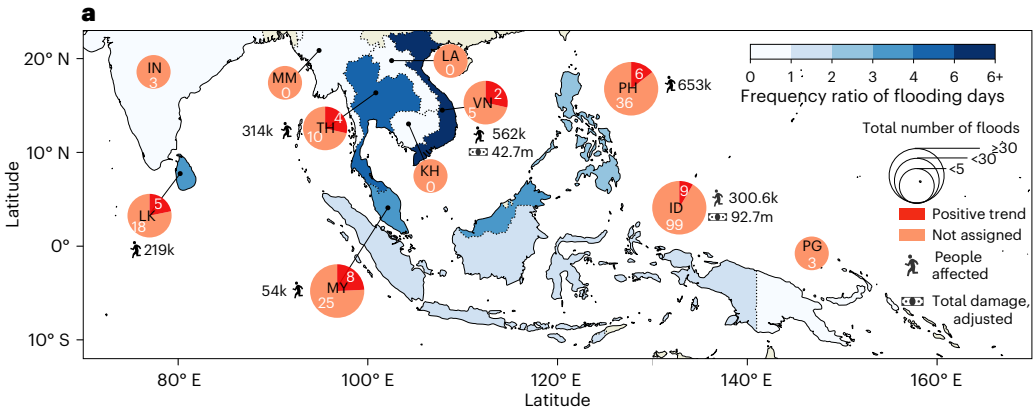

b

	All countries	TH	PH	VN	LK	MY	ID	IN	PG	KH	MM	LA
Flooding days	886 (22.3%)	107 (3.0%)	189 (4.8%)	46 (1.2%)	126 (3.2%)	218 (5.5%)	452 (11.4%)	16 (0%)	22 (0.1%)	0	0	0
Flooding days (emerging)	77 (59.2%)	21 (16.2%)	18 (13.8%)	11 (8.5%)	13 (10.0%)	28 (21.5%)	25 (19.2%)	0 (0%)	0 (0%)	0	0	0
Frequency ratio	2.65	6.00	2.91	7.30	3.15	3.92	1.69	0	0	–	–	–

Total number of DJF days (1979–2022): 3,971; emerging patterns: 130

Fig. 3 | Impact of emerging weather patterns over the tropical Indo-Pacific region according to floods recorded in the EM-DAT database. a, The ratio of DJF flood days recorded under emerging weather patterns, compared with climatology. The sizes of the pie charts represent the total floods per country from 1979 to 2022, with red slices representing floods linked to emerging weather patterns and orange slices for those not assigned. TH, Thailand; PH, Philippines; VN, Vietnam; LK, Sri Lanka; MY, Malaysia; ID, Indonesia; IN, India; PG, Papua New Guinea; KH, Cambodia; MM, Myanmar; LA, Laos. **b**, The total number of flooding days within the DJF season for each country, the flood days associated with emerging weather patterns and the respective frequency ratios.

Role of interannual variability

In the previous sections, we have shown that in the tropical Indo-Pacific region, a set of weather patterns is appearing more frequently and seem to favour specific weather extremes, while a set of weather patterns less favourable to weather extremes is gradually disappearing. Yet given that ENSO is the main driver modulating weather patterns in the region, the interplay between the identified long-term occurrence trends and ENSO, and more broadly, the contribution of interannual variability remain unclear.

In this section, we adopt a surrogate data strategy to understand the potential role of various interannual variabilities. To achieve this, we randomly shuffled the original daily ERA5 reanalysis data while maintaining intact the phases (positive, negative and neutral) of different modes of variability as illustrated in Extended Data Fig. 8a (Methods). This allows us to create scenarios where the long-term trend in ERA5 does not exist, while retaining the modulation by interannual variability.

The results indicate that the trend and coherent anomalies of TCWV over Southeast Asia and Niño 4 region (red and blue bounding boxes in Extended Data Fig. 8e) presented in Fig. 1 are robust with respect to surrogate data. Specifically, we cannot reproduce the number of emerging/disappearing patterns along with similar coherent anomaly as obtained on ERA5 (Extended Data Fig. 8c–f). For AMO and PDO, only a few patterns exhibiting trends can be identified, and their similar zero-centred anomaly distributions suggest these patterns appear to be random, indicating a weak modulation of the occurrence trend of weather patterns in this region by the AMO and PDO. Yet the surrogate data that retain ENSO and IOD variability exhibit more emerging and disappearing patterns than the other two modes of variability. However, they both yield mean anomalies that are opposite to those of the ERA5 data, suggesting that the trends identified in this study cannot be fully attributed to ENSO and IOD.

These results collectively indicate that the trends we observe cannot be fully explained by interannual variability alone. We note that the studied region also encompasses two important climate systems: the Madden–Julian Oscillation and the Asian monsoon system. These systems have been observed to exhibit long-term variations over the past few decades[42,43], which may also impact the weather patterns we have identified. However, due to their relatively higher frequency and complex coupling with interannual variability[44,45], our study is currently unable to assess the association between these systems and the observed trends in our analysis, and such an evaluation is beyond the scope of this study.

Besides modulating the occurrence trends of weather patterns, it is widely recognized that interannual variability such as ENSO also contributes substantially to weather extremes in the studied region[46]. Given the rarity of emerging weather patterns, it is still uncertain whether they can explain extremes to an extent comparable to interannual variability, or whether their contribution is negligible. To address this point, we assess the relative contributions of emerging weather patterns and ENSO to the three different types of weather extremes in the studied region.

We focus on the period 2001–2022, which contains the majority of the emerging patterns. We categorize all days within this period into six categories on the basis of their occurrence during ENSO (positive or negative phase) only, emerging patterns only, ENSO (positive or negative phase) in conjunction with emerging patterns, or they do not occur in any of the previous five cases (see the lower panel in Fig. 4). Similarly, we classify extreme events into six categories following the same definitions (see the upper panels in Fig. 4). By definition, the lower pie chart depicts the distribution of all days across the six categories considered, whereas the upper pie charts show the distribution of extreme weather days within the same categories. Hence, by comparing the lower and upper pie charts, we immediately

https://doi.org/10.1038/s41561-024-01537-8

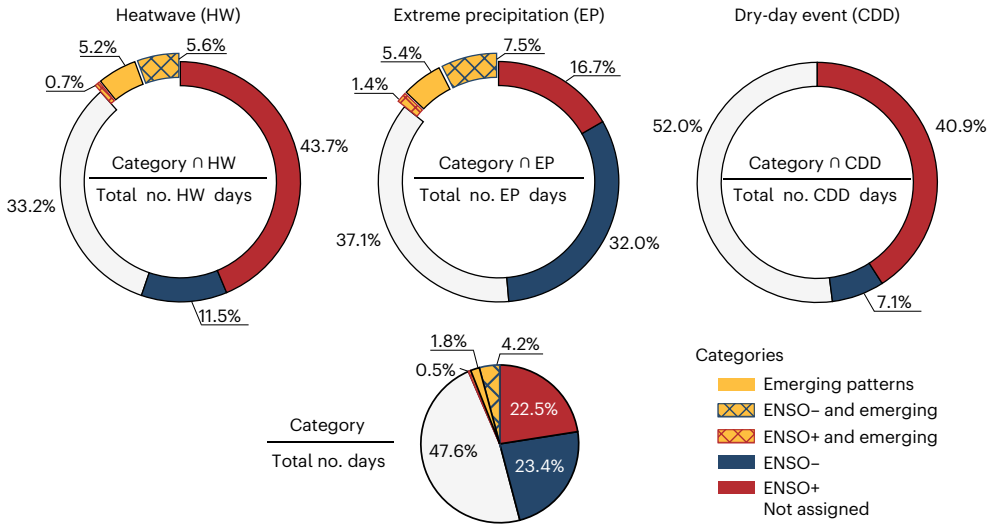

Fig. 4 | Comparative analysis of extreme weather across ENSO phases and emerging patterns in DJF. The percentages depicted in the upper pie charts are for heatwaves (left), extreme precipitation (centre) and consecutive dry days (right). More specifically, the upper pie charts show the percentages of extreme weather days for each category considered, namely ENSO positive (red), ENSO negative (blue), emerging patterns (yellow), emerging patterns and ENSO positive (yellow with red hatching), emerging patterns and ENSO negative (yellow with blue hatching) and none of the previous five categories (white), with respect to the total number of extreme weather days. The lower pie chart displays the percentages of days belonging to each of the six categories with respect to the total number of days in the period considered.

observe how the percentage of emerging patterns associated with weather extremes is notably larger than the overall percentage of emerging patterns for heatwaves (Fig. 4, top left panel) and extreme precipitation (Fig. 4, top centre panel). This shows that the emerging patterns identified are strongly linked to heatwaves and extreme precipitation in the region, and known ENSO-driven variability can only partially explain these weather extremes. If we look at how heatwaves and extreme precipitation are distributed with respect to ENSO variability, we note that heatwaves are explained largely by El Niño (red portion of the pie chart in the top left panel of Fig. 4) and extreme precipitation by La Niña (blue portion of the pie chart in the top centre panel of Fig. 4). Yet the emerging patterns explain a disproportionately large percentage of both categories of weather extremes. Remarkably, emerging patterns during La Niña phases are associated with a relatively large percentage of heatwaves, ~ 5.6%, accounting for 32.7% (5.6%/(5.6 + 11.5)%) of heatwaves during La Niña, despite accounting for only 15.2%(4.2%/(4.2 + 23.4)%) of the total La Niña days.

For consecutive dry-day events, the emerging patterns are not associated with any event at all, which is consistent with our finding that the emerging weather patterns are bringing wetter conditions.

We perform the same analysis just outlined for three other relevant modes of variability—IOD, PDO and AMO (Extended Data Fig. 9)—finding similar conclusions as the ones obtained for ENSO; these modes of variability show even weaker modulation of weather extremes than ENSO. We present the results for the other three seasons in the Supplementary Information Section 3. We additionally show the distribution of emerging and disappearing patterns with respect to the phases of each mode of variability, along with frequency maps of weather extremes conditioned to different phases of each mode of variability in the Supplementary Information Sections 4 and 5, respectively. These results further corroborate that the modes of variability considered cannot reproduce the higher frequency and spatial distribution of extremes obtained for the emerging patterns identified in this work.

The preceding results show that the long-term trends identified for specific weather patterns provide a substantial contribution to the occurrence of weather extremes in the Indo-Pacific region.

A changing tropical Indo-Pacific

In this study, we provide an analogue-based methodology to understand spatio-temporal weather changes in the tropical Indo-Pacific and link them to regional occurrences of extreme events. We identify marked ongoing changes that manifest as a set of increasingly frequent weather patterns. These lead to spatially coherent anomalies across several atmospheric variables, which manifest in a stronger PWC, wetter and warmer conditions in Southeast Asia and drier conditions in the equatorial Pacific. Despite these emerging weather patterns being relatively rare (3.2% of days for DJF), they are associated with a large number of regional extremes, notably heavy precipitation and heatwaves. The robust long-term trend of these emerging patterns does not seem linked to known natural ENSO-driven variability or to the other three relevant modes of variability, the IOD, the PDO and the AMO.

The study presented relies on reanalysis datasets. These datasets have a certain number of limitations, namely, relatively short time series as well as time-varying data assimilation strategies and observations. To address these points, we run an extensive sensitivity study that is presented in Supplementary Information Section 1, where we show that the results are consistent across reanalysis datasets and data assimilation strategies. However, the relatively short period spanned by the reanalyses prevents analysing modes of variability that have a longer period than the available reanalysis data. Notwithstanding these limitations, the results presented in this work capture changes in weather patterns in the tropical Indo-Pacific, which are aggravating regional weather extremes, using state-of-the-art reanalysis data.

Online content

Any methods, additional references, Nature Portfolio reporting summaries, source data, extended data, supplementary information, acknowledgements, peer review information; details of author contributions and competing interests; and statements of data and code availability are available at https://doi.org/10.1038/s41561-024-01537-8.

References

1. IPCC: Summary for Policymakers. In: *Climate Change 2021: The Physical Science Basis* (eds Masson-Delmotte V. et al.) (Cambridge Univ. Press, 2021).

2. Armstrong McKay, D. I. et al. Exceeding 1.5 °C global warming could trigger multiple climate tipping points. *Science* **377**, eabn7950 (2022).
3. Coronese, M., Lamperti, F., Keller, K., Chiaromonte, F. & Roventini, A. Evidence for sharp increase in the economic damages of extreme natural disasters. *Proc. Natl Acad. Sci. USA* **116**, 21450–21455 (2019).
4. Hsiang, S. M., Meng, K. C. & Cane, M. A. Civil conflicts are associated with the global climate. *Nature* **476**, 438–441 (2011).
5. Hoegh-Guldberg, O. et al. Coral reefs under rapid climate change and ocean acidification. *Science* **318**, 1737–1742 (2007).
6. Yusuf, A. A. & Francisco, H. *Climate Change Vulnerability Mapping for Southeast Asia* (Economy and Environment Program for Southeast Asia, Singapore, 2009).
7. Li, X.-X., Yuan, C. & Hang, J. Heat wave trends in Southeast Asia: comparison of results from observation and reanalysis data. *Geophys. Res. Lett.* **49**, e2021GL097151 (2022).
8. Zhang, L., Chen, Z. & Zhou, T. Human influence on the increasing drought risk over Southeast Asian monsoon region. *Geophys. Res. Lett.* **48**, e2021GL093777 (2021).
9. Phan-Van, T. et al. Drought over Southeast Asia and its association with large-scale drivers. *J. Clim.* **35**, 4959–4978 (2022).
10. Dong, Z. et al. Heatwaves in Southeast Asia and their changes in a warmer world. *Earths Future* **9**, e2021EF001992 (2021).
11. Caesar, J. et al. Changes in temperature and precipitation extremes over the Indo-Pacific region from 1971 to 2005. *Int. J. Climatol.* **31**, 791–801 (2011).
12. Faranda, D., Messori, G., Jezequel, A., Vrac, M. & Yiou, P. Atmospheric circulation compounds anthropogenic warming and impacts of climate extremes in Europe. *Proc. Natl Acad. Sci. USA* **120**, e2214525120 (2023).
13. Vautard, R. et al. Heat extremes in western Europe increasing faster than simulated due to atmospheric circulation trends. *Nat. Commun.* **14**, 6803 (2023).
14. Collins, M. et al. Challenges and opportunities for improved understanding of regional climate dynamics. *Nat. Clim. Change* **8**, 101–108 (2018).
15. Bonfils, C. J. et al. Relative contributions of mean-state shifts and ENSO-driven variability to precipitation changes in a warming climate. *J. Clim.* **28**, 9997–10013 (2015).
16. Chung, E.-S. et al. Reconciling opposing walker circulation trends in observations and model projections. *Nat. Clim. Change* **9**, 405–412 (2019).
17. L'Heureux, M. L., Lee, S. & Lyon, B. Recent multidecadal strengthening of the Walker circulation across the tropical Pacific. *Nat. Clim. Change* **3**, 571–576 (2013).
18. Power, S. et al. Decadal climate variability in the tropical Pacific: characteristics, causes, predictability, and prospects. *Science* **374**, eaay9165 (2021).
19. England, M. H. et al. Recent intensification of wind-driven circulation in the Pacific and the ongoing warming hiatus. *Nat. Clim. Change* **4**, 222–227 (2014).
20. Ma, S. & Zhou, T. Robust strengthening and westward shift of the tropical Pacific Walker circulation during 1979–2012: a comparison of 7 sets of reanalysis data and 26 CMIP5 models. *J. Clim.* **29**, 3097–3118 (2016).
21. Kociuba, G. & Power, S. B. Inability of CMIP5 models to simulate recent strengthening of the Walker circulation: implications for projections. *J. Clim.* **28**, 20–35 (2015).
22. Seager, R. et al. Strengthening tropical Pacific zonal sea surface temperature gradient consistent with rising greenhouse gases. *Nat. Clim. Change* **9**, 517–522 (2019).
23. Callahan, C. W. et al. Robust decrease in El Niño/Southern Oscillation amplitude under long-term warming. *Nat. Clim. Change* **11**, 752–757 (2021).
24. Sobel, A. H. et al. Near-term tropical cyclone risk and coupled Earth system model biases. *Proc. Natl Acad. Sci. USA* **120**, e2209631120 (2023).
25. Tangang, F. et al. Multi-model projections of precipitation extremes in Southeast Asia based on CORDEX-Southeast Asia simulations. *Environ. Res.* **184**, 109350 (2020).
26. Faranda, D., Messori, G. & Yiou, P. Dynamical proxies of North Atlantic predictability and extremes. *Sci. Rep.* **7**, 41278 (2017).
27. Falasca, F. & Bracco, A. Exploring the tropical Pacific manifold in models and observations. *Phys. Rev. X* **12**, 021054 (2022).
28. Hersbach, H. et al. The ERA5 global reanalysis. *Q. J. R. Meteorol. Soc.* **146**, 1999–2049 (2020).
29. Kobayashi, S. et al. The JRA-55 reanalysis: general specifications and basic characteristics. *J. Meteorol. Soc. Jpn II* **93**, 5–48 (2015).
30. Saha, S. et al. The NCEP climate forecast system reanalysis. *Bull. Am. Meteorol. Soc.* **91**, 1015–1058 (2010).
31. Poli, P. et al. ERA-20c: an atmospheric reanalysis of the twentieth century. *J. Clim.* **29**, 4083–4097 (2016).
32. Compo, G. P. et al. The twentieth century reanalysis project. *Q. J. R. Meteorol. Soc.* **137**, 1–28 (2011).
33. Feba, F., Ashok, K. & Ravichandran, M. Role of changed Indo-Pacific atmospheric circulation in the recent disconnect between the Indian summer monsoon and ENSO. *Clim. Dyn.* **52**, 1461–1470 (2019).
34. Saji, N. & Yamagata, T. Possible impacts of Indian Ocean dipole mode events on global climate. *Clim. Res.* **25**, 151–169 (2003).
35. Mantua, N. J. & Hare, S. R. The Pacific decadal oscillation. *J. Oceanogr.* **58**, 35–44 (2002).
36. Knight, J. R., Folland, C. K. & Scaife, A. A. Climate impacts of the Atlantic multidecadal oscillation. *Geophys. Res. Lett.* **33**, 17 (2006).
37. Sohn, B., Yeh, S.-W., Schmetz, J. & Song, H.-J. Observational evidences of Walker circulation change over the last 30 years contrasting with GCM results. *Clim. Dyn.* **40**, 1721–1732 (2013).
38. Held, I. M. & Soden, B. J. Robust responses of the hydrological cycle to global warming. *J. Clim.* **19**, 5686–5699 (2006).
39. Li, Z., Chao, Y. & McWilliams, J. C. Computation of the streamfunction and velocity potential for limited and irregular domains. *Mon. Weather Rev.* **134**, 3384–3394 (2006).
40. Delforge, D. et al. EM-DAT: The Emergency Events Database. *Preprint* https://doi.org/10.21203/rs.3.rs-3807553/v1 (2023).
41. Gall, M., Borden, K. A. & Cutter, S. L. When do losses count? Six fallacies of natural hazards loss data. *Bull. Am. Meteorol. Soc.* **90**, 799–810 (2009).
42. Roxy, M. et al. Twofold expansion of the Indo-Pacific warm pool warps the MJO life cycle. *Nature* **575**, 647–651 (2019).
43. Turner, A. G. & Annamalai, H. Climate change and the South Asian summer monsoon. *Nat. Clim. Change* **2**, 587–595 (2012).
44. Tang, Y. & Yu, B. MJO and its relationship to ENSO. *J. Geophys. Res. Atmos.* **113**, D14 (2008).
45. Ju, J. & Slingo, J. The Asian summer monsoon and ENSO. *Q. J. R. Meteorol. Soc.* **121**, 1133–1168 (1995).
46. Villafuerte, M. Q. & Matsumoto, J. Significant influences of global mean temperature and ENSO on extreme rainfall in Southeast Asia. *J. Clim.* **28**, 1905–1919 (2015).

[1]College of Design and Engineering, National University of Singapore, Singapore, Singapore. [2]Laboratoire des Sciences du Climat et de l'Environnement, UMR8212 CEA-CNRS-UVSQ, IPSL and University Paris Saclay, Gif-sur-Yvette, France. [3]Department of Earth Sciences, Uppsala University, Uppsala, Sweden. [4]Swedish Centre for Impacts of Climate Extremes (climes), Uppsala University, Uppsala, Sweden. [5]Department of Meteorology and Bolin Centre for Climate Research, Stockholm University, Stockholm, Sweden. [6]Bullard Laboratories, Department of Earth Sciences, University of Cambridge, Cambridge, UK. [7]Istituto Nazionale di Geofisica e Vulcanologia, Rome, Italy. [8]Laboratoire de Météorologie Dynamique - IPSL, ENS, PSL Research University, École Polytechnique, Institut Polytechnique de Paris, Sorbonne Université, CNRS, Paris, France. [9]Lamont-Doherty Earth Observatory, Columbia University, Palisades, NY, USA. [10]The Abdus Salam International Center for Theoretical Physics, Trieste, Italy. [11]World Meteorological Organization (WMO), Geneva, Switzerland. [12]European Centre for Medium-Range Weather Forecasts (ECMWF), Reading, UK. [13]Centre for Climate Research Singapore (CCRS), Singapore, Singapore. [14]London Mathematical Laboratory, London, UK. ✉e-mail: mpegim@nus.edu.sg

Methods

Occurrence trend analysis for weather patterns

The computation of trends in tropical atmospheric pattern analogues (also referred to as 'occurrence trends') is obtained using as observable the daily TCWV data from the ERA5 reanalysis over the period 1 January 1940 to 31 December 2022 (30,316 days). Other observables have also been used to corroborate the results found. The data adopted have horizontal resolution of 0.25° × 0.25°, and the analysis is restricted to 120° W–50° E and 20° S–20° N. This corresponds to the tropical region, spanning from eastern Africa to the western coast of North America, with a size of 381 (longitude) × 81 (latitude) = 30,861 grid points.

The underlying methodology adopted to compute occurrence trends closely follows refs. 12,26, and the six steps required are reported here for the readers' convenience.

(1) The first step is to select daily longitude–latitude maps of our observables (for example, TCWV), which we deem important for tropical atmospheric dynamics and thermodynamics.
(2) The second step consists of computing the Euclidean distance between daily maps, where we take each map as a reference state and compute its distance from all other maps in the dataset. Here we use Euclidean distance as the evaluation metric because it has been proved to be an effective measure of similarity between atmospheric weather maps in previous research[26]. We then define a high-quantile q to select the atmospheric pattern analogues. We chose $q = 0.98$, meaning that we take as analogues the 2% closest fields to the target. We describe in the following how the sensitivity to the choice of q is tested.
(3) The third step consists of dividing the time interval of 83 years into periods. We then count how many analogues N fall in each period τ, obtaining $N(\tau)$ where τ is the period chosen. For this analysis, we chose 9 periods of approximately 9 years. Further analyses have shown that shortening these periods will not change our results qualitatively.
(4) The fourth step is to perform a linear fit of $N(\tau)$ of the type $a\tau + b$. Using a cubic fit does not qualitatively affect the results (not shown here).
(5) The fifth step is to estimate the upper and lower 95% confidence intervals (CIs) of the a parameter of the fit using the Wald method[47]. If the lower and the upper bounds of the CI for a are positive (negative), we interpret this as a significant positive (negative) trend for the selected daily observable map and quantile q. If the confidence interval contains zero, the trend is non-significant.
(6) The sixth step consists of repeating the preceding five steps for $q = 0.99$ and $q = 0.995$. We retain as daily maps with significant increasing (decreasing) occurrence trends only those having consistent (same sign and significant) occurrence trends for all three quantiles. These are the robust weather patterns that are analysed in this paper. We additionally verify that the quality (distance) of analogues for these patterns is comparable to that for all other days in our dataset.

We adopted 95% CIs as boundaries for statistical significance, which means a 5% probability of the actual trend lying outside the CI range. Given that CIs are symmetric intervals, this implies that the likelihood of the 'true' trend having an opposite direction is ≤2.5%. In practice, since we select only for weather patterns that exhibit significant trends for three different quantiles q simultaneously, the chance of selecting inappropriate patterns is negligible.

The methodology just described is used to identify the emerging and disappearing patterns depicted in Fig. 1. In particular, the trends mentioned for emerging and disappearing patterns are shown in Fig. 1k,l, respectively, where we display the distribution of analogues for each period. Figure 1i,j shows the temporal distribution of emerging and disappearing patterns (vertical bars), respectively, as well as their seasonality (pie chart). The remaining Fig. 1a–h depicts the composite anomalies for the emerging and disappearing weather patterns, which are further described later in the 'Computation of composite anomalies maps' section of Methods.

Computation of composite anomalies maps

We produce composite anomalies for the days displaying significant occurrence trends for several daily variables: TCWV, 850 hPa stream-function and wind, daily total precipitation and 2 m temperature. The data were processed to remove a grid-point by grid-point linear trend for the whole analysis period. This ensures that the composite anomaly maps are not affected by the occurrence time of those weather patterns. The data were further deseasonalized using a mean seasonal cycle computed by averaging over the same calendar days. Geographical anomalies' significance is assessed through a bootstrap procedure (sample size of 500) that involves randomly selecting a number of days equal to the days in each composite from the entire dataset, regardless of their trend. Anomalies are considered significant if they fall below the fifth percentile or above the 95th percentile of the bootstrap distribution for each grid point.

Surrogate data generated by random shuffling

Since the emerging patterns in our study are rare and resembling, to a certain extent, La Niña-like patterns, we investigate whether the identified trends are driven by internal variability. To this end, we use surrogate data, generated by maintaining the internal variability within the dataset while eliminating the trends. To achieve this, we perform random shuffling conditioned to the phase of each mode of variability considered, as shown in Extended Data Fig. 8a. In particular, we first classify all weather patterns into three phases of a given internal mode of variability on the basis of thresholds set at the 25th and 75th percentiles of the associated climate index. Then we randomly shuffle the weather patterns within each phase to create one surrogate dataset. For each internal variability considered in our study, including ENSO, IOD, PDO and AMO, we generate 2,000 surrogate datasets. Finally, we apply the occurrence trend analysis to all reshuffled datasets and identify weather patterns exhibiting significant occurrence trends. The results are shown in Extended Data Fig. 8b–f.

Extracting extreme events from reanalysis dataset

In this study, we focus on three prominent types of weather extremes in the tropical Indo-Pacific: heatwaves, extreme precipitation and consecutive dry days. Those extremes are extracted on each individual grid point from the ERA5 reanalysis data from 1979 to 2022, using the following definitions.

(1) Heatwave: we adopt TX90pct as a relative threshold to define heatwaves in our study[48]. The threshold for one day at one grid point is the calendar-day 90th percentile of the daily maximum temperature, based on a centred 15 day window. A heatwave is defined as three or more consecutive days exceeding this threshold, and all days belonging to this heatwave are considered as heatwave days for that grid point.
(2) Extreme precipitation: we define extreme precipitation as days with daily precipitation exceeding the 95th percentile on wet days with daily precipitation greater than 1 mm (ref. 49).
(3) Consecutive dry days: consecutive dry-day events are defined as a period of five or more consecutive days with daily precipitation less than 1 mm. All days belonging to this consecutive dry-day event are considered as consecutive dry days[49].

When defining extremes, we remove a grid-point by grid-point long-term trend from the the data. This is because we want to maintain a relatively uniform distribution of extremes in the studied period. Using data with trends leads to the identification of more frequent

heatwaves and extreme precipitation in recent decades, where our emerging patterns cluster. This might raise the question of whether the extremes associated with emerging weather patterns are polluted by the underlying climate trend. Thus, removing the long-term trend effectively prevents overestimation of our results, although it probably underestimates the impact brought by these emerging patterns, given that heatwaves and extreme precipitation in the region are reported to be more frequent and intense[7].

To investigate and compare the contribution of emerging weather patterns and various modes of variability to weather extremes, we further define extreme events as days on which a minimum number of grid points are identified as extremes. Specifically, extreme events are identified as days when the number of grid points classified as extreme exceeds the top 10th percentile. We further apply this method of defining extremes to smaller regions using regional land masks (Supplementary Tables 1 and 2). The computation of the overall spatial frequency effectively excludes point-wise patches, increasing the robustness of the results. After identifying these daily extreme events, we classified them into six categories on the basis of their Niño3.4 index (≥75th percentile of Niño3.4, ≤25th percentile of Niño3.4, 25th to 75th percentile of Niño3.4) and whether they are associated with emerging weather patterns: La Niña only, El Niño only, emerging patterns only, emerging patterns belonging to La Niña, emerging patterns belonging to El Niño, and not assigned to ENSO or emerging patterns. In our study, the phases of other modes of variability are defined using the same threshold criteria applied to each mode's respective index.

Frequency ratio maps

In this study, the frequency ratio maps are presented to show whether our identified weather patterns are more/less favouring the occurrence of extremes. First, we calculate the frequency of extreme events across the overall period for each season. More specifically, this is computed counting the number of extreme days divided by the total number of days on a grid-point by grid-point basis. Then we assess the frequency of extremes occurring during emerging/disappearing weather patterns within the corresponding season. This is calculated as the ratio between the number of extremes occurring during emerging patterns and the total number of emerging patterns (also in this case on a grid-point by grid-point basis). These steps produce two frequency maps. The frequency ratio map is then derived by dividing the frequency map of extremes under emerging and disappearing weather patterns by the frequency map of extremes not conditioned by emerging and disappearing patterns.

Impacts of floods associated with emerging patterns

We take floods from the EM-DAT[40]. We focus on events over Southeast Asia, India and Sri Lanka, excluding those floods where no start and/or end day was provided, and dates included in several events were counted only once. We consider only floods that occurred between 1979 and 2022 here, which matches the period used for reanalysis data, as this helps maintain consistency in the study and avoids the periods for which EM-DAT lacks comprehensive records. For floods lasting more than 10 days, only the first 10 days are considered as flooding days since for prolonged floods, their mechanisms may be more complex and cannot be attributed simply to specific weather patterns. Following these criteria, from 1,189 floods recorded in the region of interest, we identified 2,843 flooding days over 698 floods. We further divide these flooding days by season and country and calculate their frequency ratio of flooding days in different countries during different seasons, specifically DJF (Fig. 3), March–April–May (Supplementary Fig. 8), June–July–August (Supplementary Fig. 9) and September–October–November (Supplementary Fig. 10).

To determine whether a given flood is associated with emerging weather patterns, we check whether the fraction of days with emerging weather patterns within the event is higher than the occurrence frequency of emerging weather patterns in climatology. If so, it is then considered as one of the associated events. We claim that this is likely to underestimate the impact of emerging weather patterns since flooding might exhibit a certain delay relative to extreme precipitation, depending on many factors such as topography, soil saturation, drainage systems and more. Following the preceding definition, Fig. 3 and Supplementary Figs. 8, 9 and 10 collectively show the number of floods that are associated with emerging weather patterns in different seasons. These figures also detail the specific distributions of those identified floods across different countries, along with the number of people affected and the economic losses incurred.

Data availability

The ERA5 reanalysis data used in this study are available at https://cds.climate.copernicus.eu/#!/search?text=ERA5&type=dataset. The NCEP reanalysis data are from https://psl.noaa.gov/data/gridded/data.ncep.reanalysis.html. The JRA55, 20CR and ERA-20C are from the Climate Data Guide (https://climatedataguide.ucar.edu/). The climate indices for ENSO, IOD, AMO and PDO are publicly available at climate explorer (http://climexp.knmi.nl/). The impact data for flooding events are available from https://www.emdat.be/.

Code availability

The code used for the analysis and visualization is available at https://doi.org/10.5281/zenodo.13172443 (ref. 50).

References

47. Stein, C. & Wald, A. Sequential confidence intervals for the mean of a normal distribution with known variance. *Ann. Math. Stat.* **18**, 427–433 (1947).
48. Perkins, S., Alexander, L. & Nairn, J. Increasing frequency, intensity and duration of observed global heatwaves and warm spells. *Geophys. Res. Lett.* **39**, 20 (2012).
49. Folland, C. et al. Workshop on indices and indicators for climate extremes, Asheville, NC, USA, 3–6 June 1997 breakout group c: temperature indices for climate extremes. *Climatic Change* **42**, 31–43 (1999).
50. Dong, C. Indo-Pacific regional extremes aggravated by changes in tropical weather patterns. *Zenodo* https://doi.org/10.5281/zenodo.13172443 (2024).

Acknowledgements

We thank J. Wei for providing valuable advice on the design of the figures presented in this paper. This work is supported by Singapore's MOE Tier 2 Grant MOE-T2EP50221-0006: 'Prediction-to-Mitigation with Digital Twins of the Earth's Weather', the ANR-20-CE01-0008-01 (SAMPRACE) grant, Swedish Research Council Vetenskapsrådet grant no. 2022-06599, the European Union's Horizon 2020 research and innovation programme under grant agreement no. 101003469 (XAIDA), state aid managed by the National Research Agency under France 2030 bearing the reference no. ANR-22-EXTR-0005 (TRACCS-PC4-EXTENDING project) and the 'COESION' project funded by the French National programme LEFE (Les Enveloppes Fluides et l'Environnement).

Author contributions

G. Mengaldo and D.F. conceived the study. D.F., C.D., G. Messori, R.N., G. Mengaldo, C.C. and A.G. contributed to the design of the methodology. C.D. and G. Mengaldo performed the analysis and wrote the original draft based on discussions with R.N., G. Messori, A.G., L.F., P.Y., M.V., F.D., S.J.C., E.C., G.B., C.C. and D.F. All authors discussed the results and contributed to writing and editing the paper.

Competing interests
The authors declare no competing interests.

Additional information
Extended data is available for this paper at https://doi.org/10.1038/s41561-024-01537-8.

Supplementary information The online version contains supplementary material available at https://doi.org/10.1038/s41561-024-01537-8.

Correspondence and requests for materials should be addressed to Gianmarco Mengaldo.

Peer review information *Nature Geoscience* thanks Phan Van Tan, Jérôme Vialard and the other, anonymous, reviewer(s) for their contribution to the peer review of this work.

https://doi.org/10.1038/s41561-024-01537-8

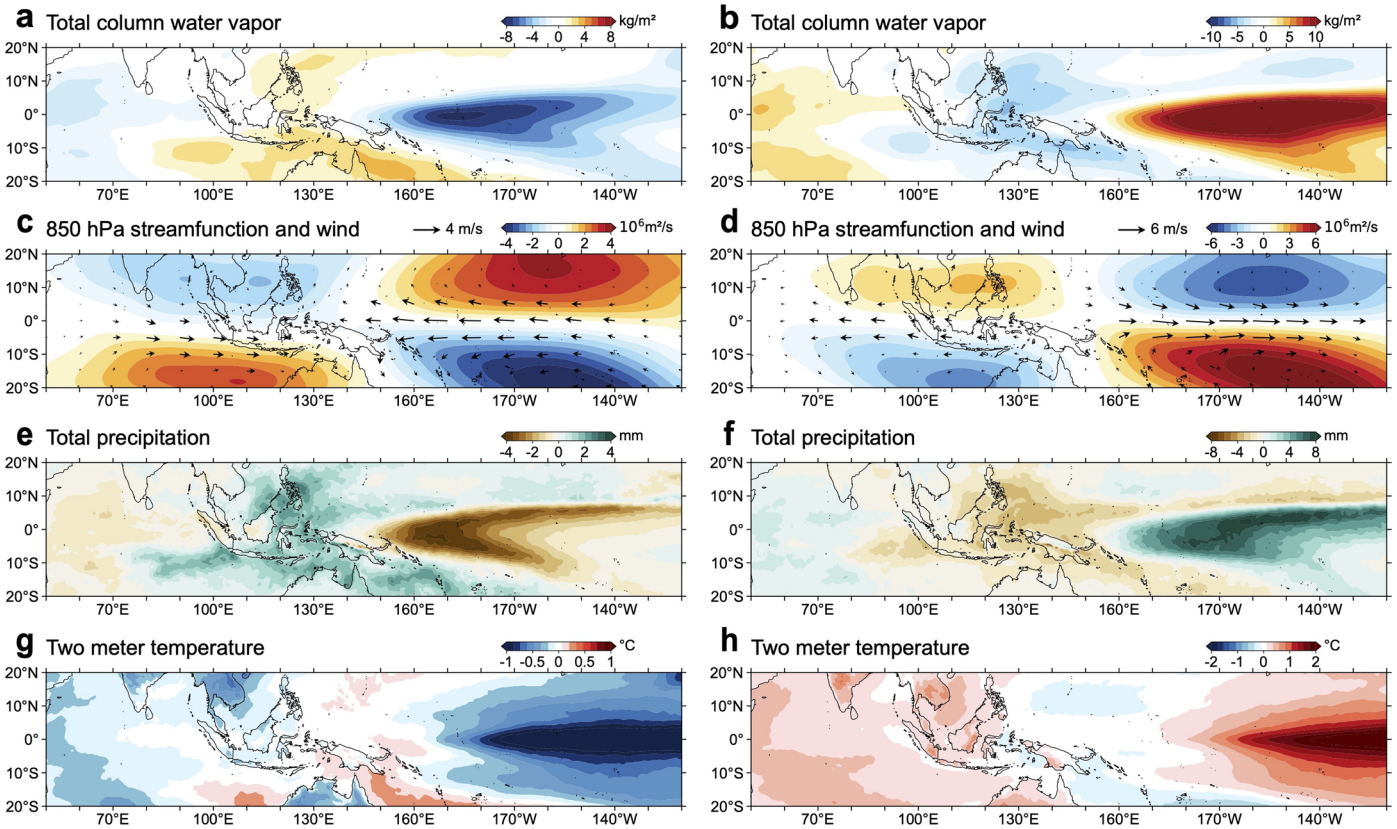

Extended Data Fig. 1 | Composite anomalies conditioned by the Niño3.4 index. The left column (**a**,**c**,**e**,**g**) depicts composite anomalies of La Niña, obtained using data with Niño3.4 index less than -1.5. The right column (**b**,**d**,**f**,**h**) depicts composite anomalies of El Niño, obtained using data with Niño3.4 index greater than 1.5.

https://doi.org/10.1038/s41561-024-01537-8

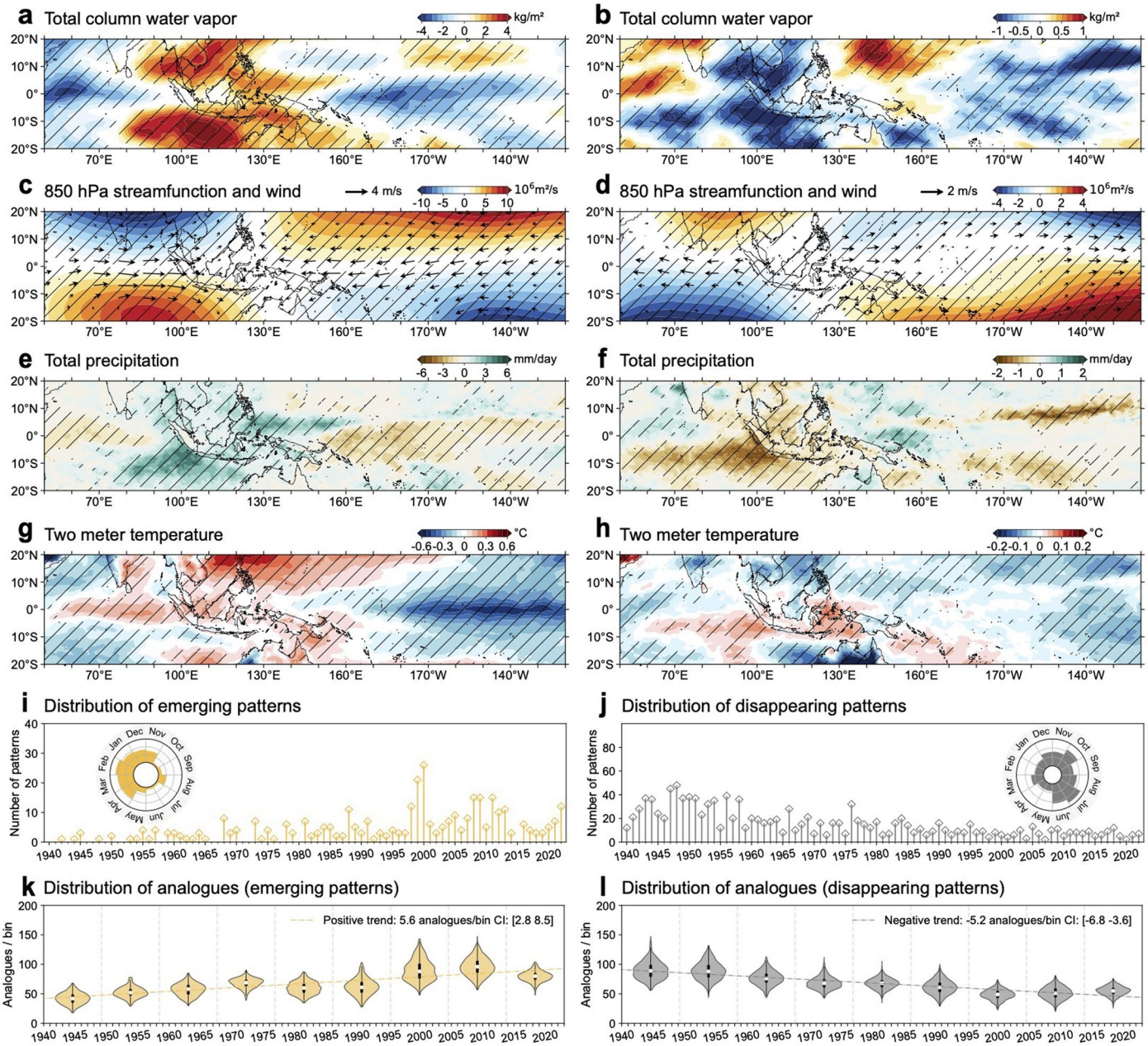

Extended Data Fig. 2 | Composite anomalies (a–h), for patterns with significant occurrence trends (i,j), and associated analogues (k,l), using the 850hPa streamfunction as observable. As in Fig. 1, but the observable used for occurrence trend analysis is the 850hPa streamfunction instead of TCWV. The ends of the boxes represent the 25th and 75th percentiles, with the whiskers extending up to 1.5 times the interquartile range beyond the box. The white dot in each box shows the medians (n=353 for emerging patterns, n=1278 for disappearing patterns).

https://doi.org/10.1038/s41561-024-01537-8

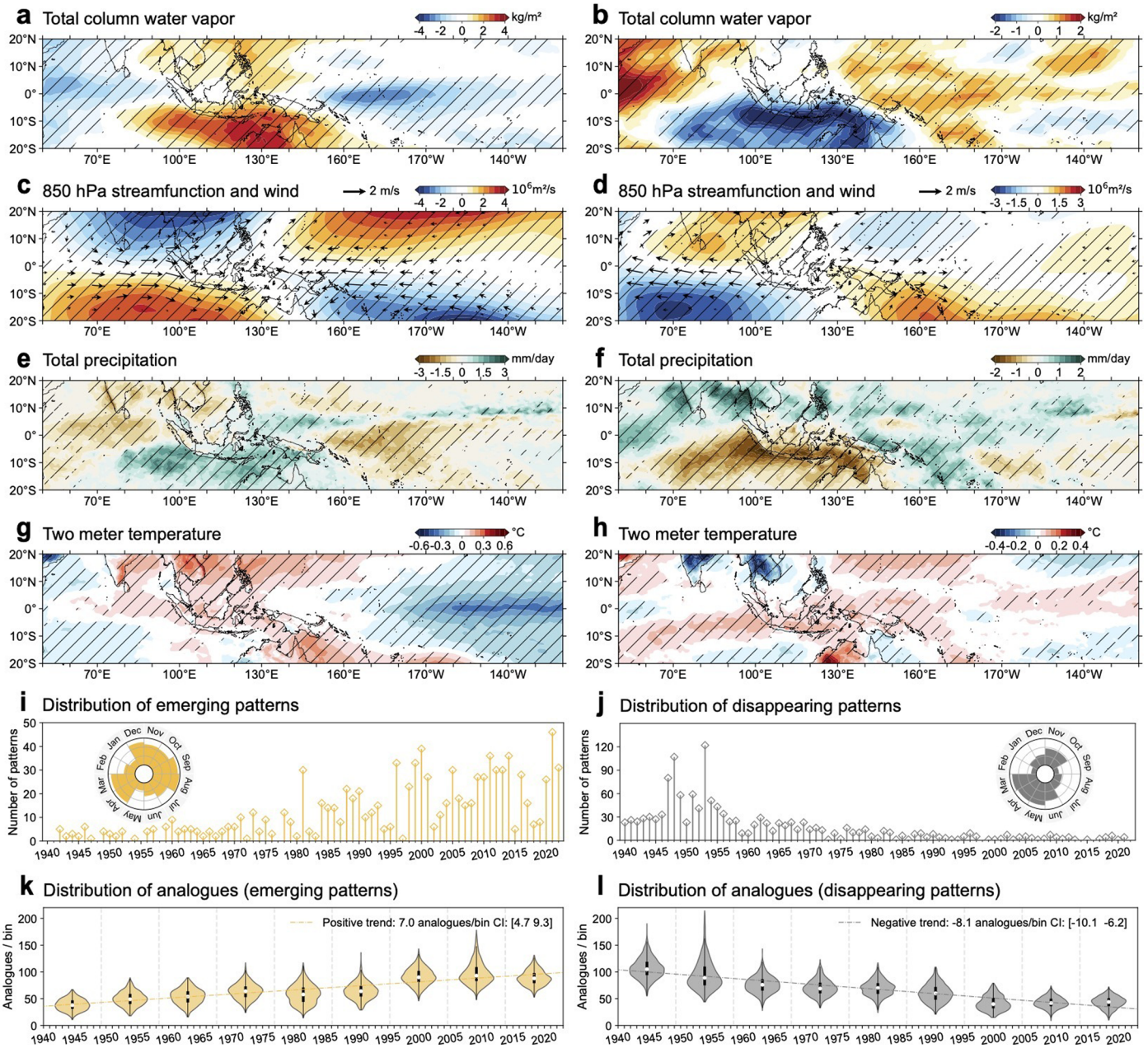

Extended Data Fig. 3 | Composite anomalies (a–h), for patterns with significant occurrence trends (i,j), and associated analogues (k,l), using the 200hPa streamfunction as observable. As in Fig. 1, but the observable used for occurrence trend analysis is the 200hPa streamfunction instead of TCWV. The ends of the boxes represent the 25th and 75th percentiles, with the whiskers extending up to 1.5 times the interquartile range beyond the box. The white dot in each box shows the medians (n=978 for emerging patterns, n=1323 for disappearing patterns).

https://doi.org/10.1038/s41561-024-01537-8

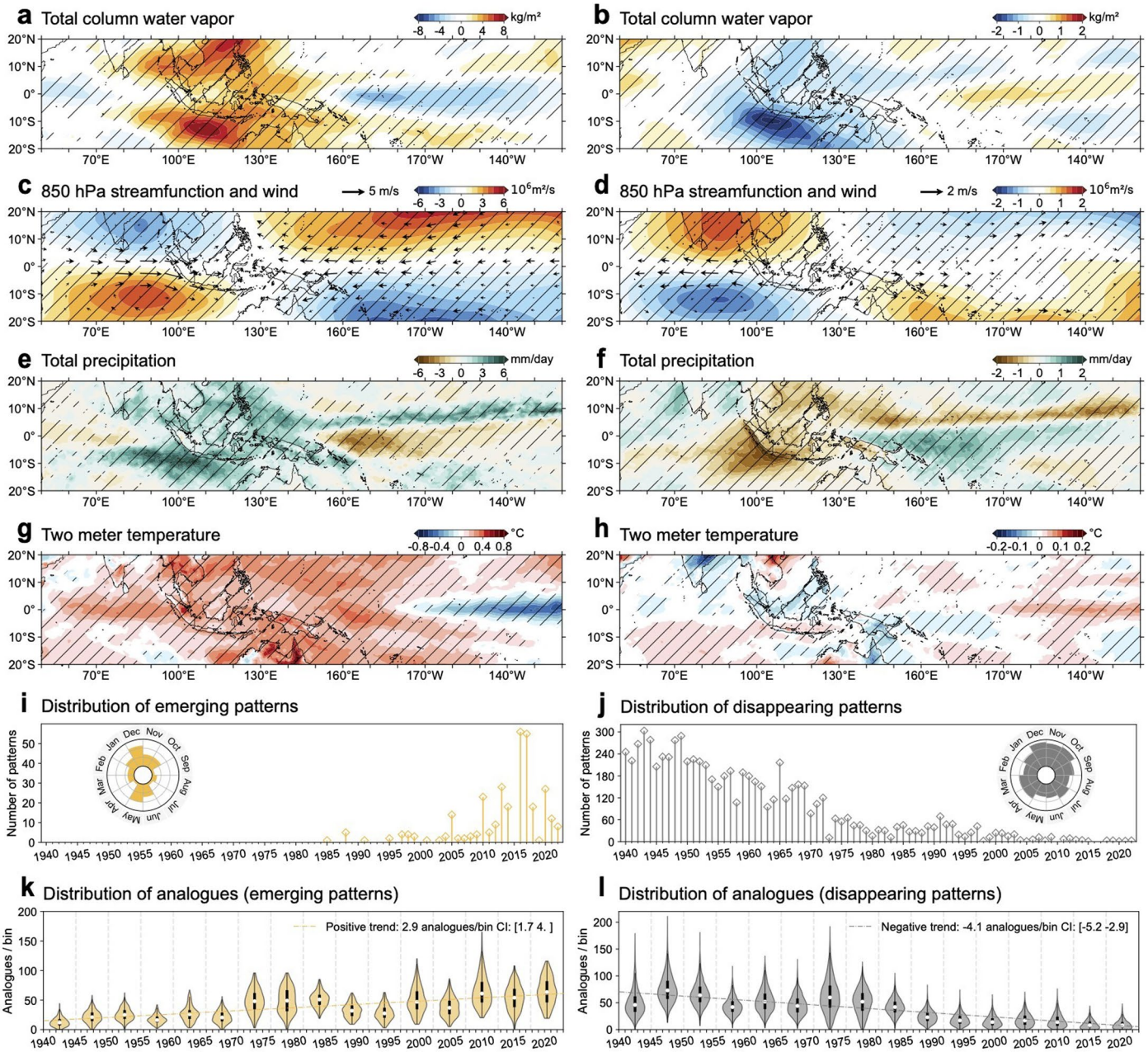

Extended Data Fig. 4 | Composite anomalies (a–h), for patterns with significant occurrence trends (i,j), and associated analogues (k,l), using TCWV as observable, and 16 time periods. As in Fig. 1, but the number of time periods used for occurrence trend analysis is 16 instead of 9. The ends of the boxes represent the 25th and 75th percentiles, with the whiskers extending up to 1.5 times the interquartile range beyond the box. The white dot in each box shows the medians (n=310 for emerging patterns, n=7287 for disappearing patterns).

https://doi.org/10.1038/s41561-024-01537-8

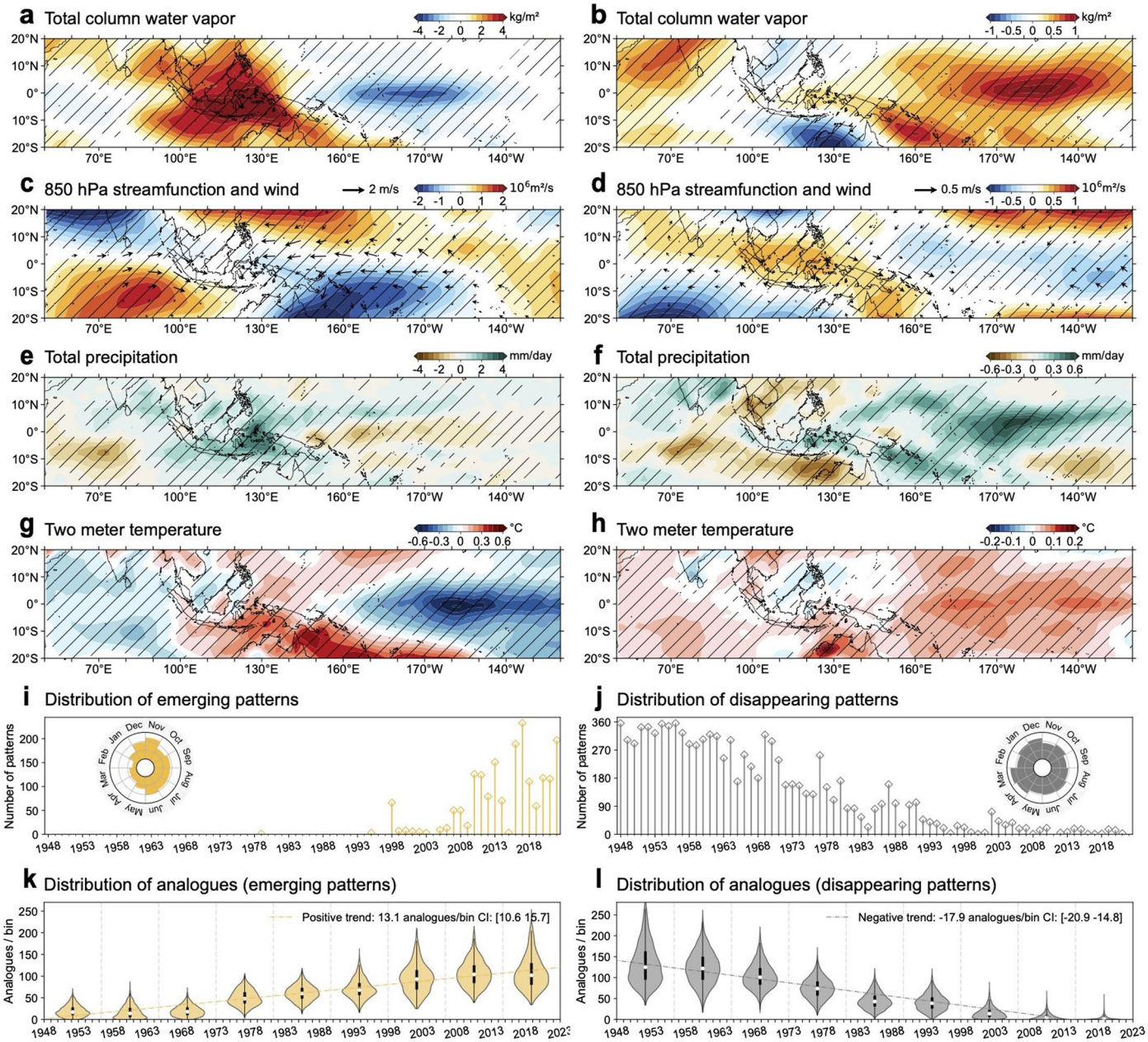

Extended Data Fig. 5 | Composite anomalies (a–h), for patterns with significant occurrence trends (i,j), and associated analogues (k,l). As in Fig. 1, but for the NCEP reanalysis dataset. The ends of the boxes represent the 25th and 75th percentiles, with the whiskers extending up to 1.5 times the interquartile range beyond the box. The white dot in each box shows the medians (n=1814 for emerging patterns, n=9939 for disappearing patterns).

https://doi.org/10.1038/s41561-024-01537-8

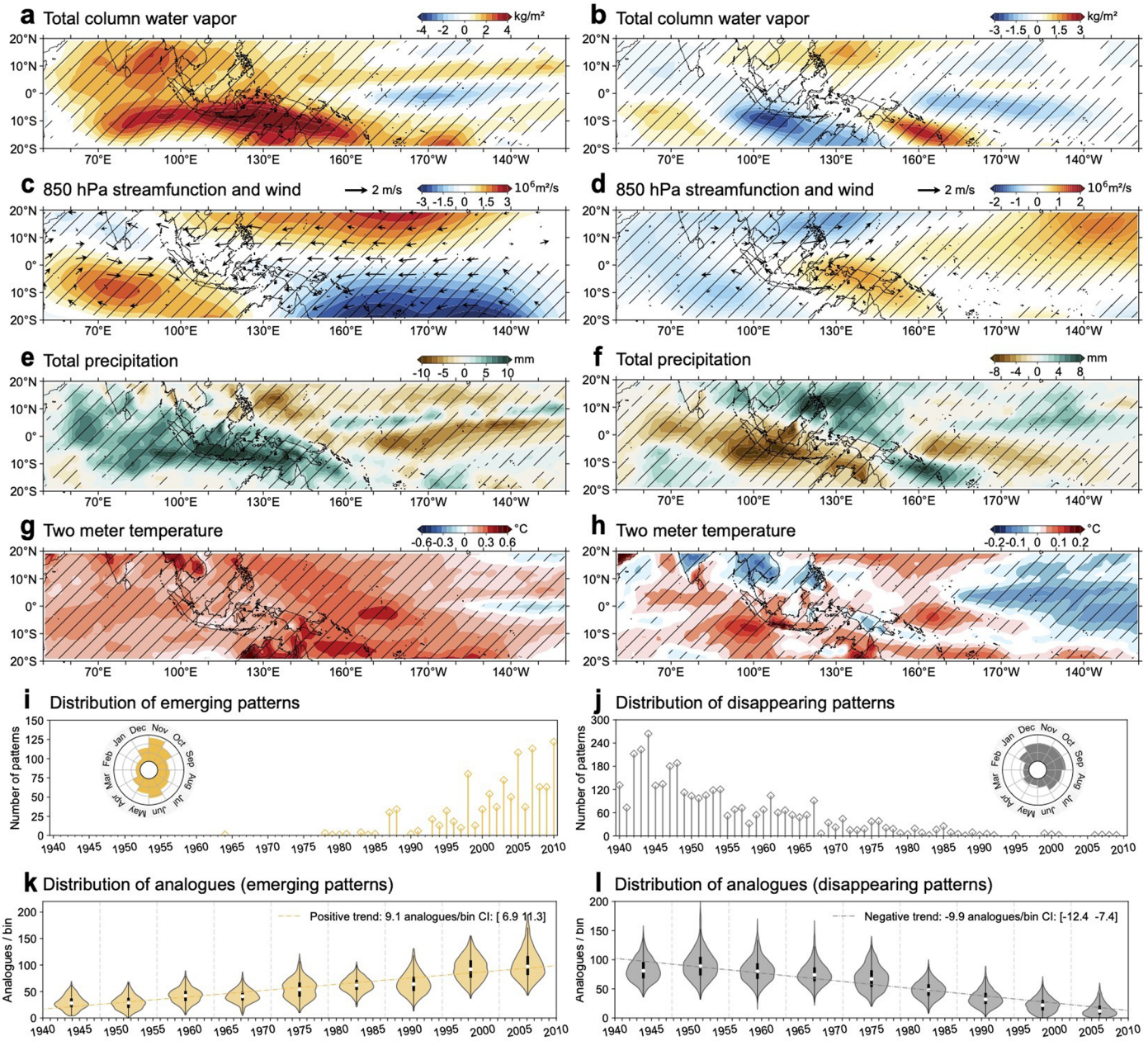

Extended Data Fig. 6 | Composite anomalies (a–h), for patterns with significant occurrence trends (i,j), and associated analogues (k,l), using TCWV as observable. As in Fig. 1, but for the ERA-20C reanalysis dataset. The ends of the boxes represent the 25th and 75th percentiles, with the whiskers extending up to 1.5 times the interquartile range beyond the box. The white dot in each box shows the medians (n=1027 for emerging patterns, n=3419 for disappearing patterns).

https://doi.org/10.1038/s41561-024-01537-8

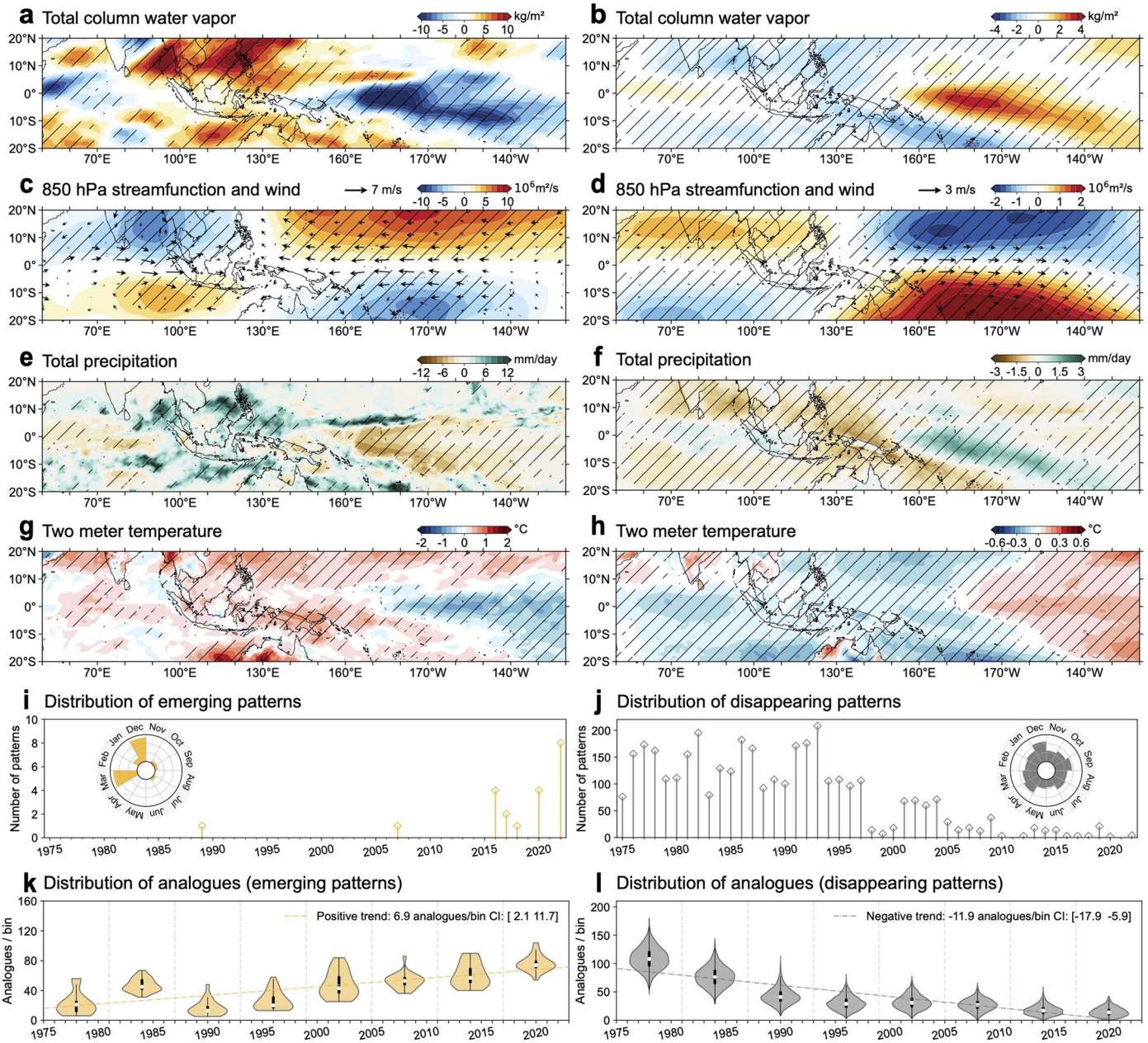

Extended Data Fig. 7 | Composite anomalies (a–h), for patterns with significant occurrence trends (i,j), and associated analogues (k,l), using TCWV as observable, and the last 48 years. As in Fig. 1, but for the last 48 years (from 1975 to 2022) to verify the sensitivity with respect to the satellite observation era. The number of time periods used for occurrence trend analysis in this shorter time history is equal to 8. The ends of the boxes represent the 25th and 75th percentiles, with the whiskers extending up to 1.5 times the interquartile range beyond the box. The white dot in each box shows the medians (n=21 for emerging patterns, n=17532 for disappearing patterns).

https://doi.org/10.1038/s41561-024-01537-8

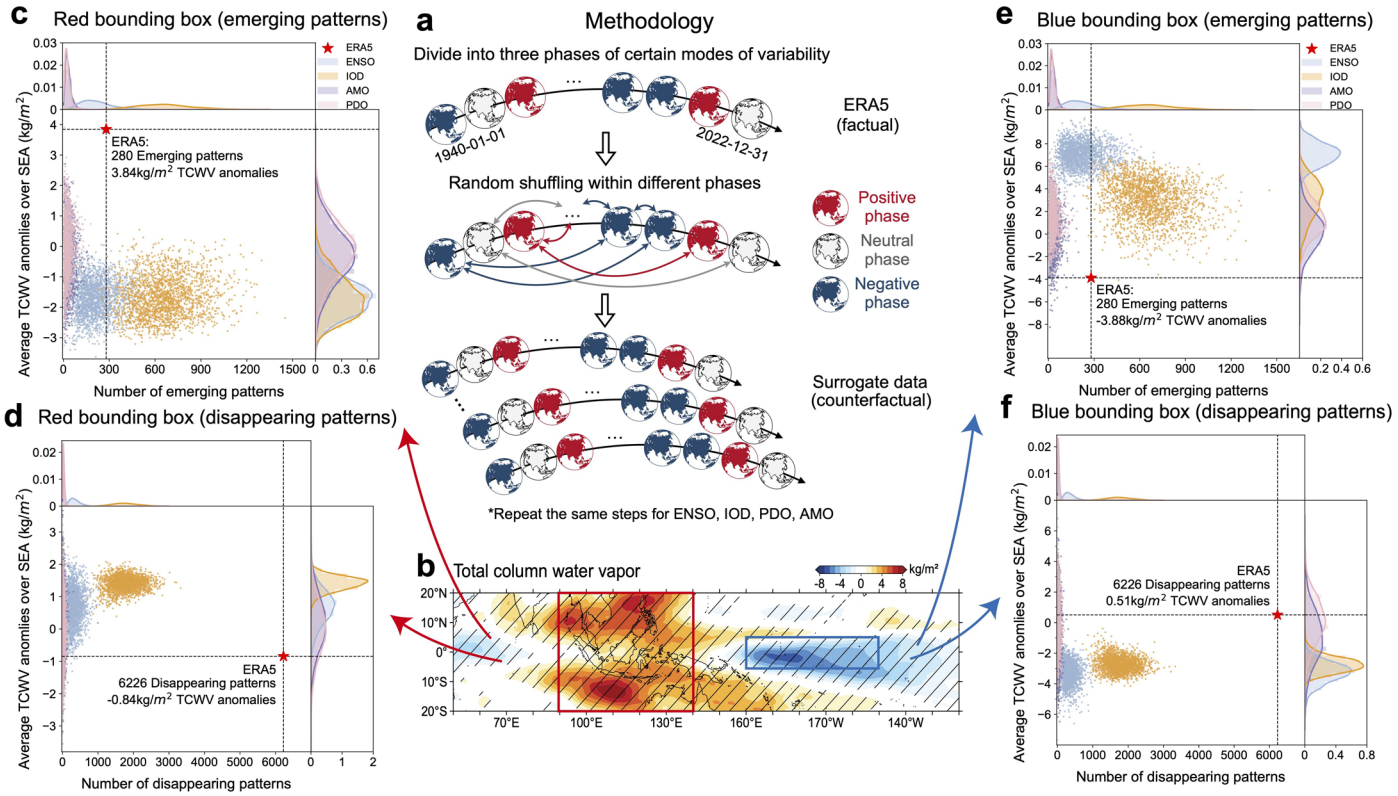

Extended Data Fig. 8 | Surrogate data study of the trend analysis. Plot (**a**) depicts a schematic representation of the framework for generating surrogate data through random shuffling of data applied within each phase (positive, neutral, negative) of each mode of variability considered in this study, that is, ENSO, IOD, AMO and PDO. The three colors of the Earth correspond to three different phases of a mode of variability, that is, red being positive, white neutral, and blue negative. The scatter plots (**c**,**d**,**e**,**f**) display results obtained from surrogate data for emerging patterns (**c**,**e**) and disappearing patterns (**d**,**f**), for the four modes of variability considered, and the result obtained on the original non-reshuffled data, red star. In (**c**) and (**d**), the average total column water vapor anomaly is computed within the red bounding box (90E-140E, 20N–20S) shown in (**b**), while for (**e**) and (**f**), it is derived from the blue bounding box (160E-150W, 5N–5S). Figure (b) displays composite anomalies of emerging patterns obtained from the ERA5 reanalysis dataset, identical to Fig. 1(a), with the bounding boxes used for calculating the TCWV anomaly.

https://doi.org/10.1038/s41561-024-01537-8

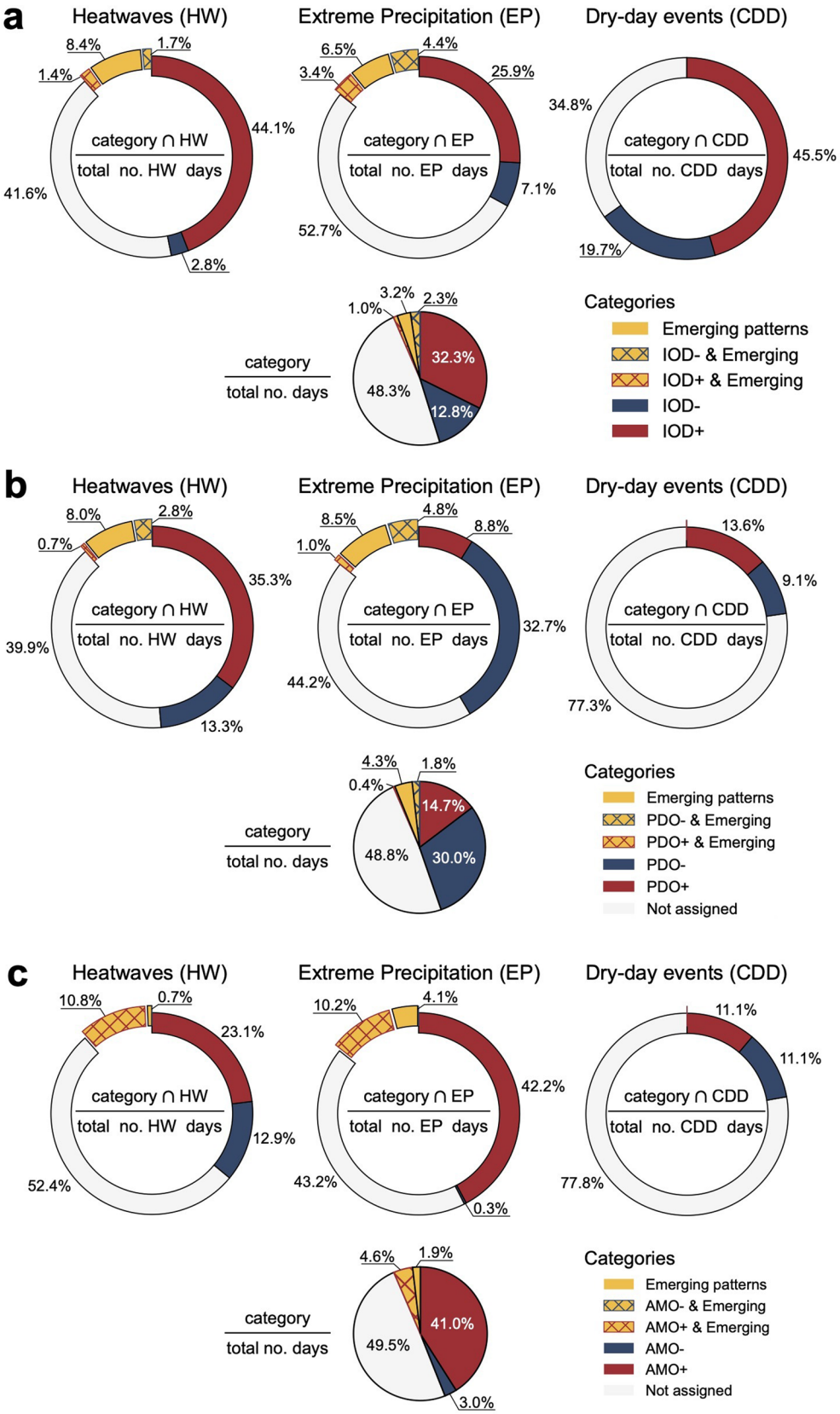

Extended Data Fig. 9 | Percentages of extreme weather events during positive (red) and negative (blue) phases of internal variability, and during emerging patterns (yellow), for DJF. As in Fig. 4, but for the IOD (**a**), PDO (**b**), and AMO (**c**).

https://doi.org/10.1038/s41561-024-01537-8

Extended Data Table 1 | Occurrence trends analysis for different observables

	Occurrence Trend	
Observable	*Positive*	*Negative*
TCWV	280 (0.92%)	6226 (20.53%)
850hPa-S	353 (1.16%)	1278 (4.22%)
200hPa-S	978 (3.23%)	1323 (4.36%)
SLP	749 (2.47%)	1213 (4.00%)
2m-T	5690 (18.77%)	8351 (27.55%)
500hPa-W	0 (0.00%)	8993 (29.66%)
TP	0 (0.00%)	17909 (59.07%)
TCC	1219 (4.02%)	1201 (3.96%)
OLR	1004 (3.31%)	1982 (6.54%)

Number of weather patterns (and associated percentage with respect to the total number of days in the dataset) with positive and negative occurrence trends identified for different observables, using the ERA5 reanalysis dataset in the period 1940-2022.